JACS
JOURNAL OF THE AMERICAN CHEMICAL SOCIETY
pubs.acs.org/JACS
Article

Enhanced Photocurrent of All-Inorganic Two-Dimensional Perovskite $Cs_2PbI_2Cl_2$ via Pressure-Regulated Excitonic Features

Songhao Guo, Kejun Bu, Jiangwei Li, Qingyang Hu, Hui Luo, Yihui He, Yanhui Wu, Dongzhou Zhang, Yongsheng Zhao, Wenge Yang, Mercouri G. Kanatzidis, and Xujie Lü*

Cite This: J. Am. Chem. Soc. 2021, 143, 2545−2551

ABSTRACT: Pressure processing is efficient to regulate the structural and physical properties of two-dimensional (2D) halide perovskites which have been emerging for advanced photovoltaic and light-emitting applications. Increasing numbers of studies have reported pressure-induced and/or enhanced emission properties in the 2D halide perovskites. However, no research has focused on their photoresponse properties under pressure tuning. It is also unclear how structural change affects their excitonic features, which govern the optoelectronic properties of the halide perovskites. Herein, we report significantly enhanced photocurrents in the all-inorganic 2D perovskite $Cs_2PbI_2Cl_2$, achieving over 3 orders of magnitude increase at the industrially achievable level of 2 GPa in comparison with its initial photocurrent. Lattice compression effectively regulates the excitonic features of $Cs_2PbI_2Cl_2$, reducing the exciton binding energy considerably from 133 meV at ambient conditions to 78 meV at 2.1 GPa. Impressively, such a reduced exciton binding energy of 2D $Cs_2PbI_2Cl_2$ is comparable to the values of typical 3D perovskites ($MAPbBr_3$ and $MAPbI_3$), facilitating the dissociating of excitons into free carriers and enhancing the photocurrent. Further pressurization leads to a layer-sliding-induced phase transition and an anomalous negative linear compression, which has not been observed so far in other halide perovskites. Our findings reveal the dramatically enhanced photocurrents in the 2D halide perovskite by regulating its excitonic features and, more broadly, provide new insights into materials design toward extraordinary properties.

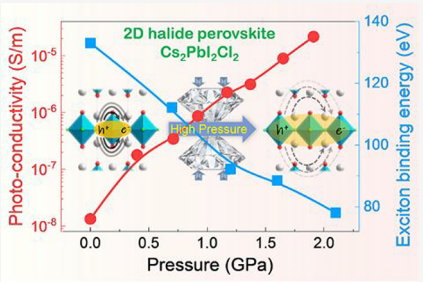

INTRODUCTION

Two-dimensional (2D) Ruddlesden−Popper (RP) perovskites, exhibiting diverse and tunable optoelectronic properties as well as superior stability, have emerged as potential alternatives to their 3D analogues for applications in high-efficiency solar cells and light-emitting diodes.[1−6] Because of strong dielectric and quantum confinements, excitons (electron−hole pairs) in 2D perovskites are stabilized even at room temperature and possess high binding energies (E_b ∼ hundreds of meV).[1,7] It is well-known that the E_b is crucial for the optoelectronic properties of the halide perovskites because it determines the probability of exciton dissociation and charge carrier recombination.[8,9] Hence, tuning the E_b of 2D halide perovskites could further enhance their performance in optoelectronic devices. Achieving these calls for a better fundamental understanding, which requires more suitable material systems as well as advanced *in situ* regulation and characterization methods.

Compared to organic−inorganic hybrid 2D perovskites, all-inorganic compounds possess higher stability and potentially lower E_b, which is attractive for photovoltaic applications.[10] A recently developed all-inorganic 2D RP perovskite $Cs_2PbI_2Cl_2$ exhibits superior characteristics, including strong photoresponse, high carrier mobility, and outstanding stability.[10] The inorganic spacer Cs^+ cations reduce the dielectric mismatch between the quantum well and barrier, providing lower shielding of the electrons and holes in the octahedron layers. Thus, a relatively weak excitonic feature exists in the all-inorganic $Cs_2PbI_2Cl_2$. More importantly, the significantly smaller interlayer distance, setting $Cs_2PbI_2Cl_2$ apart from all the hybrid 2D perovskites, enables to achieve the unexplored structural feature and provide more opportunities for both fundamental studies and performance optimization upon applying external stimuli including pressure and temperature.

Pressure processing is a powerful way to modify the physical and chemical properties of various functional materials, which furthers our fundamental understanding of structure−property relationships and also enables the discovery of novel materials otherwise unobtainable.[11−15] For example, pressure-based materials engineering has induced emergent or enhanced optoelectronic properties of semiconductive oxides, sulfides, and halides.[16−19] Recently, studies on pressure-induced variations of structures and emission properties of 2D

Received: November 9, 2020
Published: January 19, 2021

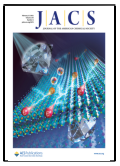

https://dx.doi.org/10.1021/jacs.0c11730
J. Am. Chem. Soc. 2021, 143, 2545−2551

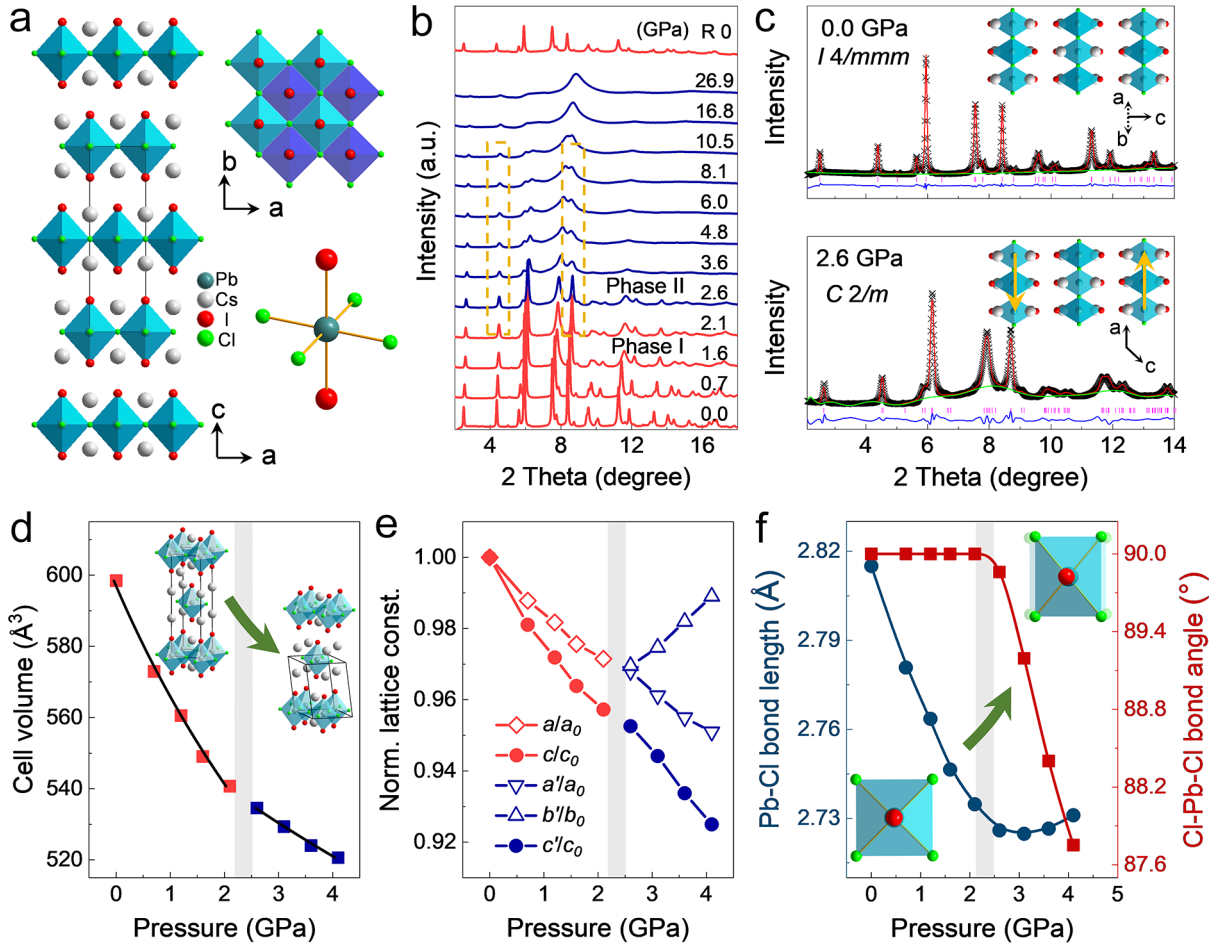

Figure 1. *In situ* structural characterizations of $Cs_2PbI_2Cl_2$ under high pressure. (a) Ambient crystal structure along different crystallographic axes and the elongated $[PbI_2Cl_4]$ octahedral unit. (b) Synchrotron XRD patterns at selected pressures. (c) Rietveld refinement results of XRD patterns collected at 0.0 and 2.6 GPa. The inset shows the corresponding crystal structure and the sliding direction. (d) Unit-cell volumes as a function of pressure fitted by Birch−Murnaghan equation of states. (e) Compressibility along different lattice axes, where $a' = \sqrt{2}a/2$, $b' = \sqrt{2}b/2$, and $c' = 2\sin(\beta)c$. (f) Pb−Cl bond length and Cl−Pb−Cl bond angle as a function of pressure.

perovskites have been growing rapidly.[20−24] However, no research has focused on their photoresponse under high pressure despite the fact that the influence of excitonic features on their optoelectronic properties is of great interest. In this work, we report the remarkably enhanced photocurrent by more than 3 orders of magnitude via pressure-tuned excitonic features in the all-inorganic 2D perovskite $Cs_2PbI_2Cl_2$. The variations of structural and physical properties have been investigated by comprehensive high-pressure characterization and theoretical calculations, demonstrating the direct link between the excitonic features and the optoelectronic properties of 2D halide perovskites.

RESULTS AND DISCUSSION

$Cs_2PbI_2Cl_2$ adopts the tetragonal structure with space group $I4/mmm$ (phase I) and lattice constants of $a = b = 5.6385(8)$ Å and $c = 18.879(4)$ Å at ambient conditions. The 2D $[PbI_2Cl_2]_n^{2n-}$ layer is built by the corner-sharing $[PbI_2Cl_4]^{4-}$ units (Figure 1a), where Cl^- and I^- anions occupy in-plane shared corners and out-of-plane terminal ligands, respectively. With the Cs^+ cations separating the layers, $Cs_2PbI_2Cl_2$ possesses a standard 2D RP-type perovskite structure.

In situ X-ray diffraction (XRD) measurements were performed to investigate the structural evolution of $Cs_2PbI_2Cl_2$ under high pressures. Figure 1b and Figure S1 exhibit the integrated XRD profiles at different pressures. Upon compression, all diffraction peaks shift to higher 2θ angles due to the lattice contraction. When the applied pressure exceeded 2.6 GPa, a structural phase transition occurs, as evidenced by the anomalous left shift of some diffraction peaks. We further conducted single-crystal XRD to identify the crystal structure of the high-pressure phase (phase II), as shown in Figure S2. At 2.8 GPa, $Cs_2PbI_2Cl_2$ adopts a monoclinic structure with space group $C2/m$, giving the lattice constants of $a = 7.749(2)$ Å, $b = 7.800(2)$ Å, $c = 9.863(14)$ Å, and $\beta = 112.29(4)°$ (Tables S1 and S2).

Interestingly, the tetragonal-to-monoclinic phase transition of $Cs_2PbI_2Cl_2$ arises from the layer sliding of the 2D $[PbI_2Cl_2]_n^{2n-}$ plane along the a-axis, which has never been observed in perovskite materials. Layer sliding could result in the exceptional phenomenon of negative linear compressibility, which has been reported in $Co(SCN)_2(pyrazine)_2$, a layered metal−organic framework.[25] In the hybrid 2D $(BA)_2(MA)_{n-1}Pb_nI_{3n+1}$, the compression process includes two steps of interlayer and intralayer dominated compression at low- and high-pressure regions, respectively.[26] As the pressure increases, the intralayer compression results in Pb−I bond length shortening and Pb−I−Pb angle narrowing, both of

https://dx.doi.org/10.1021/jacs.0c11730
J. Am. Chem. Soc. 2021, 143, 2545−2551

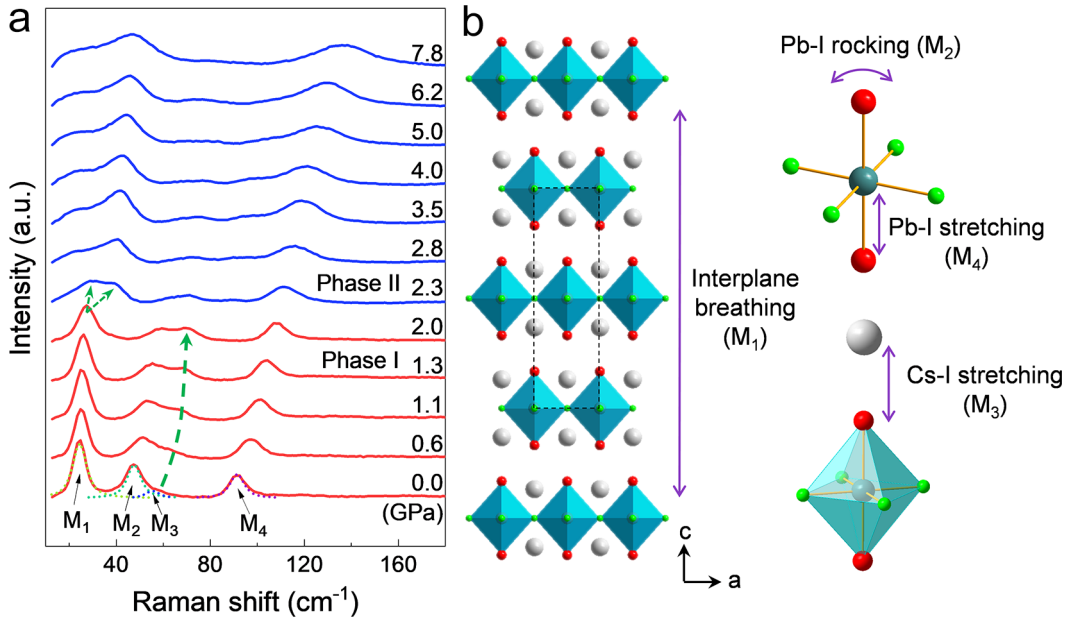

Figure 2. (a) Raman spectra of $Cs_2PbI_2Cl_2$ at different pressures. (b) Schematic representation of the vibrational modes of $Cs_2PbI_2Cl_2$.

which manifest as octahedron tilting in the hybrid 2D perovskite.[21,27,28] However, the tilting is not allowed in the all-inorganic 2D $Cs_2PbI_2Cl_2$ because of its crystallographic symmetry limitation. The polarization between I^- and Cs^+ is strong, while the interlayer van der Waals interaction is relatively weak. Therefore, when the separation distance exceeds a certain threshold, the original structure collapses, resulting in a holistic layer sliding without octahedron tilting.

The Rietveld refinement profiles for XRD data collected at different pressures are displayed in Figure 1c and Figure S3. The ambient tetragonal structure (phase I) was used to fit the patterns up to 2.1 GPa, while the monoclinic structure (phase II) was used to fit the patterns at 2.6 GPa and higher pressures. The variation of the cell volumes of $Cs_2PbI_2Cl_2$ under high pressure is displayed in Figure 1d. Using the Birch−Murnaghan equation of state to fit the pressure-dependent unit-cell volumes, bulk modulus (K_0) values of 16.8 GPa for phase I and 42.8 GPa for phase II were obtained, indicating the less compressible nature of phase II. The lattice constants for different axes of $Cs_2PbI_2Cl_2$ are displayed as a function of pressure in Figure 1e, where the anisotropic compressibility can be found in both phase I and phase II. It is worth noting that negative linear compressibility is observed in phase II, where the unit cell counterintuitively expands along the *b*-axis (perpendicular to the sliding direction *a*) accompanied by an overall volume reduction during compression. This has never been reported in halide perovskites. The calculated compressibility coefficient of the *b*-axis is $K_b = -13$ TPa^{-1}, which is typically in the range of the value from 5 to 50 TPa^{-1} for crystalline materials.[29] The negative linear compressibility arises from the anisotropic distortion of the octahedron in phase II, evidenced by the quick decrease of the Cl−Pb−Cl bond angle and a slight increase of the Pb−Cl bond length (Figure 1f). This would lead to the contraction of the octahedron along the sliding direction and expansion perpendicular to the sliding direction. When the pressure exceeded 15 GPa, the large deformation of the octahedra makes the perovskite structure unstable and amorphized.

The phase transition of $Cs_2PbI_2Cl_2$ is further confirmed by *in situ* Raman spectroscopy. As shown in Figure 2, four Raman-active modes are observed at wavenumbers of 24.4, 47.2, 52.4, and 91.6 cm^{-1}, corresponding to interplane breathing, Pb−I rocking, Cs−I stretching, and Pb−I stretching, respectively. Upon compression, all Raman peaks shift to higher frequency due to the bonds shortening. It is worth noting that the peak intensity for Cs−I stretching obviously increased before the phase transition, indicating the stronger polarization interaction between I and Cs. When the pressure exceeded 2.3 GPa, the Raman peak for interplane breathing splits into two, suggesting a breakdown of symmetry, which is in line with the XRD results.

To understand the relationship of the lattice structure and excitonic features of $Cs_2PbI_2Cl_2$, high-pressure UV−vis absorption spectra were collected (Figure 3a and Figure S4). At ambient conditions, $Cs_2PbI_2Cl_2$ exhibits a sharp absorption edge at 3.08 eV, where the kink at the absorption edge is originated from the excitonic absorption.[1,30,31] The kink becomes smaller with increasing pressure, which indicates the decrease of exciton binding energy E_b. As reported, the E_b in 2D perovskite derived from two collaborative effects: quantum confinement and dielectric confinement.[1,2] The exciton wave function is confined into the 2D plane by the quantum wells, increasing E_b; then, the barriers with low dielectric constant poorly screens the electrostatic interaction between electrons and holes, thereby further enhancing the E_b by dielectric confinement.[2,32] To evaluate the dielectric confinement in $Cs_2PbI_2Cl_2$ at different pressures, DFT calculations were performed to compute the high-frequency dielectric constants perpendicular to the layers (ε_{zz}). As shown in Figure S5, the dielectric constants continuously increase from 3.97 at ambient conditions to 4.36 at 2.1 GPa, which is mainly attributed to the shortening of the interlayer distance under high pressure (from ~3.10 Å at ambient conditions to ~2.74 Å at 2.1 GPa). Therefore, the interlayer dielectric mismatch is reduced, which suppresses the dielectric confinement of the excitons in $Cs_2PbI_2Cl_2$.

https://dx.doi.org/10.1021/jacs.0c11730
J. Am. Chem. Soc. 2021, 143, 2545−2551

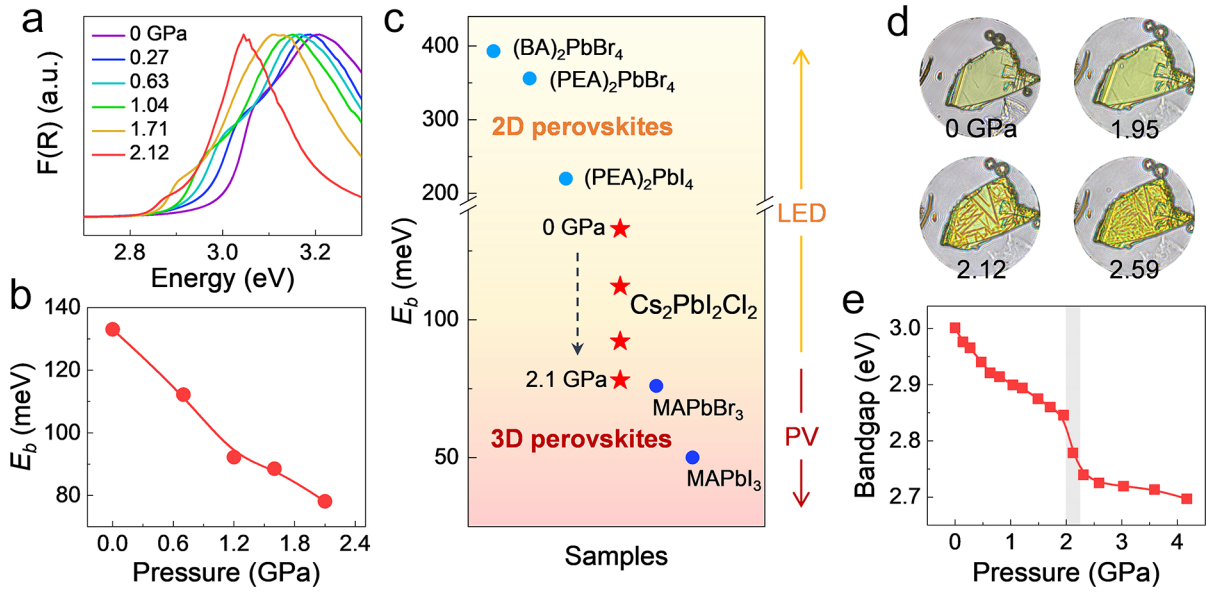

Figure 3. Optical characterizations of $Cs_2PbI_2Cl_2$ under high pressure. (a) Selected UV−vis absorption spectra upon compression, where the kink at the absorption edge is originated from the excitonic absorption. (b) Calculated exciton binding energies at different pressures. (c) The E_b value of typical 3D and 2D perovskites in comparison with those of $Cs_2PbI_2Cl_2$ under high pressure (MA = methylammonium, PEA = phenethylammoniuim, and BA = butylammonium), where the data for $(BA)_2PbBr_4$, $(PEA)_2PbBr_4$, $(PEA)_2PbI_4$, $MAPbBr_3$, and $MAPbI_3$ come from the literature.[33−35] (d) Optical micrographs collected at selected pressures, where the orange textures stem from the inhomogeneous stress distribution induced by the phase transition. (d) Bandgap as a function of pressure.

Consequently, the E_b values at different pressures are calculated according to the Wannier−Mott exciton model[36] (Supporting Information) and plotted in Figure 3b, which reveals a significant decrease from 133 meV at ambient conditions to 78 meV up to 2.1 GPa. The reduced exciton binding energy would destabilize the photogenerated excitons and make them more mobile. Figure 3c exhibits the E_b value of typical 3D and 2D perovskites in comparison with those of $Cs_2PbI_2Cl_2$ at different pressures. Impressively, the E_b value of $Cs_2PbI_2Cl_2$ at 2.1 GPa has reached the region comparable to the values of 3D halide perovskites and much lower than the representative 2D hybrid perovskites. Therefore, by applying pressure, we can regulate the excitonic feature of 2D perovskites to mimic the behavior in 3D compounds but without losing their advantages, making the 2D materials more promising for photovoltaic applications.

It is interesting that the orange textures can be observed starting from 2 GPa (Figure 3d and Figure S6). The inhomogeneous stress distribution induced by the phase transition could usually break the single crystals, and cracks or interfaces may generate.[16] The bandgap widths of $Cs_2PbI_2Cl_2$ under high pressure are plotted in Figure 3e, where a sudden drop happened at 2 GPa due to the phase transition. Theoretical calculations reveal the direct bandgap nature and a similar band structure for both phases (Figure S7). The states near the conduction band minimum (CBM) are mainly consisting of Pb-6p states, and the valence band maximum (VBM) consists of Cl-3p/I-5p and Pb-6s antibonding states.[10,37] The highly dispersive nature near the band edges of $Cs_2PbI_2Cl_2$ are credited for the outstanding in-plane carrier transport properties. By utilizing parabolic band approximation, we calculated the effective masses of both the electron and hole in $Cs_2PbI_2Cl_2$ at different pressures (Figure S8). The effective masses continually decrease upon compression, which indicates enhanced carrier mobility. The calculated pressure-dependent bandgap is exhibited in Figure S9, which is in line with experimental results. The narrowing of the bandgap during the phase transition is ascribed from the enhanced overlap of the Pb−I and Pb−Cl electron clouds by the Cl−Pb−Cl and I−Pb−Cl bonds bending (Figure 1f and Figure S10), thereby increasing the electronic band dispersion.

The key processes for photovoltaic applications include photoabsorption, charge carrier separation, and migration. $Cs_2PbI_2Cl_2$ is reported to be promising as a UV and hard radiation detector at ambient conditions due to its direct bandgap, high carrier mobility, and excellent moisture stability.[10,37] However, the performance is still limited by its relatively high E_b (133 meV) compared to k_BT (26 meV at room temperature), suggesting that the photogenerated excitons can be stabilized and hardly dissociate into free carriers. Benefiting from the reduced E_b by pressure regulation, the enhanced photoresponse is presumable. To this end, we performed an *in situ* in-plane photocurrent measurement in a $Cs_2PbI_2Cl_2$ single crystal under high pressures. As shown in Figure 4a, the photocurrents exhibit fast on−off switch responses and rapidly enhance up to 2 GPa. The corresponding photoconductivity markedly increases by more than 3 orders of magnitude to 2.2×10^{-5} S/m at 1.91 GPa compared with 1.3×10^{-8} S/m at ambient conditions (see Figure 4b). After the phase transition, and with rising pressure, the photocurrents of $Cs_2PbI_2Cl_2$ gradually decrease (Figure S11) because of the generation of interfaces and the structural amorphization, which introduce carrier scattering and additional recombination channels.[38,39]

The mechanism of photoresponse evolution in $Cs_2PbI_2Cl_2$ is illustrated in Figure 4c. The generated excitons could either be stabilized or dissociate into free carriers depending on the binding energy E_b,[40,41] making E_b one of the key parameters for optoelectronic materials.[31,42] The relatively high E_b value of $Cs_2PbI_2Cl_2$ at ambient conditions stabilizes the excitons, giving the observed excitonic feature in the absorption spectrum (Figure 3a). When the pressure reaches 2.1 GPa, the reduced

https://dx.doi.org/10.1021/jacs.0c11730
J. Am. Chem. Soc. 2021, 143, 2545−2551

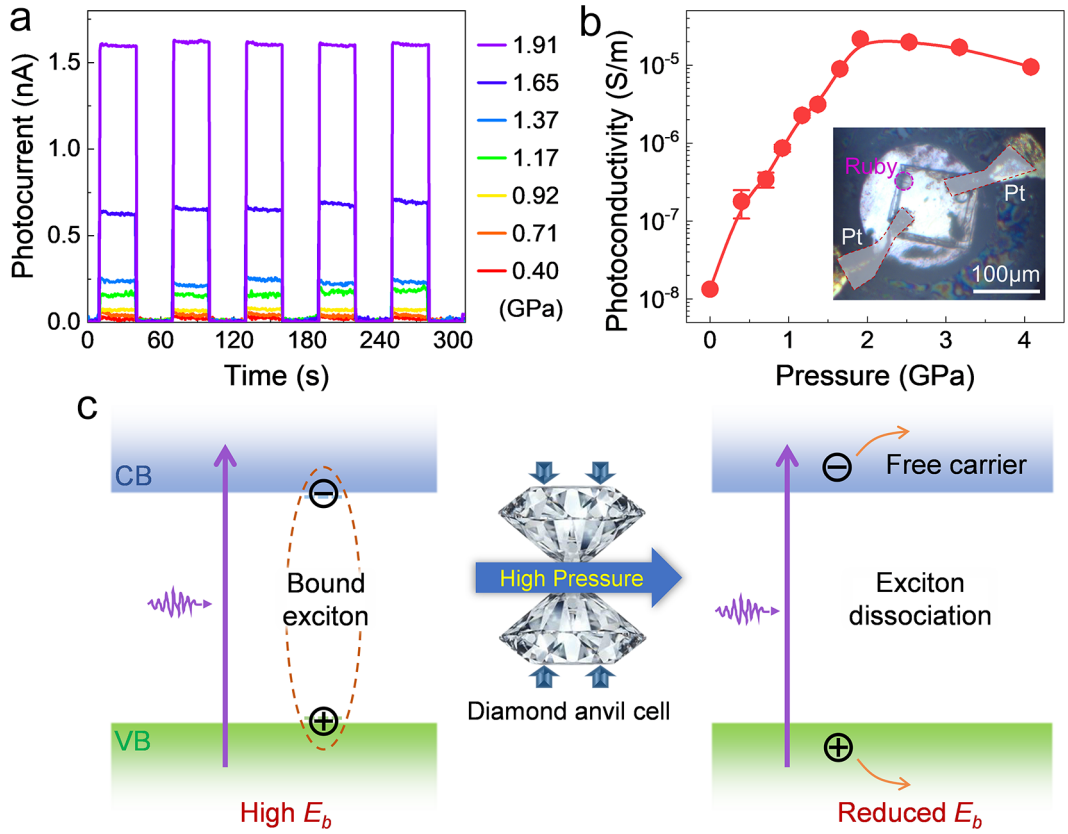

Figure 4. Photoresponse properties of $Cs_2PbI_2Cl_2$ under high pressure. (a) Photocurrents upon compression in phase I. (b) Pressure-induced evolution of photoconductivity, where the data at ambient conditions is derived from the literature.[10] The inset displays a microphotograph of the crystal with platinum probes in the diamond anvil cell. (c) Schematic diagram of the pressure-promoted exciton dissociation.

E_b is comparable to the 3D perovskites $MAPbBr_3$ and $MAPbI_3$. This means that the excitons are more likely to dissociate into free carriers, just like in the 3D compounds. Moreover, the pressure-induced higher mobility makes these free carriers easier to migrate toward current collectors. Therefore, a dramatically enhanced photoresponse in $Cs_2PbI_2Cl_2$ is achieved via the pressure-reduced excitonic feature.

CONCLUSION

Using pressure to regulate the excitonic features, we achieved remarkably enhanced photocurrents in an all-inorganic 2D halide perovskite $Cs_2PbI_2Cl_2$, reaching more than 3 orders of magnitude increment at ~2 GPa in comparison to the initial value. The dielectric confinement is greatly suppressed during compression, providing lower shielding of the Coulombic interactions between electrons and holes. Consequently, the exciton binding energy of $Cs_2PbI_2Cl_2$ decreased from 133 meV at ambient conditions to 78 meV at 2.1 GPa, reaching a value comparable to the typical 3D halide perovskites. Further compression induces a tetragonal-to-monoclinic phase transition that arises from the sliding of the octahedron layers. Intriguingly, an unusual negative linear compression phenomenon was revealed in the high-pressure phase of $Cs_2PbI_2Cl_2$ due to the contraction of the octahedron along the sliding direction but expansion perpendicular to the sliding direction, which has never been reported in halide perovskites.

ASSOCIATED CONTENT

Supporting Information

The Supporting Information is available free of charge at https://pubs.acs.org/doi/10.1021/jacs.0c11730.

Experimental details, crystallographic data, lattice parameters, XRD patterns, Rietveld refinements, reflectance spectra, dielectric constants, optical images, band structures, and effective masses (PDF)

Accession Codes

CCDC 2055130 contains the supplementary crystallographic data for this paper. These data can be obtained free of charge via www.ccdc.cam.ac.uk/data_request/cif, or by emailing data_request@ccdc.cam.ac.uk, or by contacting The Cambridge Crystallographic Data Centre, 12 Union Road, Cambridge CB2 1EZ, UK; fax: +44 1223 336033.

AUTHOR INFORMATION

Corresponding Author

Xujie Lü – *Center for High Pressure Science and Technology Advanced Research (HPSTAR), Shanghai 201203, China;* orcid.org/0000-0001-8402-7160; Email: xujie.lu@hpstar.ac.cn

Authors

Songhao Guo – *Center for High Pressure Science and Technology Advanced Research (HPSTAR), Shanghai 201203, China*

Kejun Bu – *Center for High Pressure Science and Technology Advanced Research (HPSTAR), Shanghai 201203, China*

https://dx.doi.org/10.1021/jacs.0c11730
J. Am. Chem. Soc. 2021, 143, 2545−2551

Jiangwei Li − *Key Lab of Organic Optoelectronics, Molecular Engineering of Ministry of Education, Department of Chemistry, Tsinghua University, Beijing 100084, China;* orcid.org/0000-0002-4089-1747
Qingyang Hu − *Center for High Pressure Science and Technology Advanced Research (HPSTAR), Shanghai 201203, China;* orcid.org/0000-0002-2742-3017
Hui Luo − *Center for High Pressure Science and Technology Advanced Research (HPSTAR), Shanghai 201203, China*
Yihui He − *Department of Chemistry, Northwestern University, Evanston, Illinois 60208, United States;* orcid.org/0000-0002-1057-6826
Yanhui Wu − *Center for High Pressure Science and Technology Advanced Research (HPSTAR), Shanghai 201203, China*
Dongzhou Zhang − *Hawaii Institute of Geophysics & Planetology, University of Hawaii Manoa, Honolulu, Hawaii 96822, United States*
Yongsheng Zhao − *Center for High Pressure Science and Technology Advanced Research (HPSTAR), Shanghai 201203, China*
Wenge Yang − *Center for High Pressure Science and Technology Advanced Research (HPSTAR), Shanghai 201203, China*
Mercouri G. Kanatzidis − *Department of Chemistry, Northwestern University, Evanston, Illinois 60208, United States;* orcid.org/0000-0003-2037-4168

Complete contact information is available at: https://pubs.acs.org/10.1021/jacs.0c11730

Funding

This work was supported by the National Nature Science Foundation of China (NSFC) (Grants U1930401, 51527801, and 17N1051-0213). J.L. was supported by the National Natural Science Foundation of China (Grant 91433205), Tsinghua University Initiative Scientific Research Program. Q.H was supported by a XPLORE Award. At Northwestern work was supported by the U.S. Department of Energy, Office of Science, Basic Energy Sciences, under Grant SC0012541 (compound synthesis and characterization). GeoSoilEnviro-CARS was supported by the National Science Foundation - Earth Sciences (EAR-1634415), Department of Energy GeoSciences (DE-FG02−94ER14466), and partially by COMPRES under NSF Cooperative Agreement EAR-1606856. Use of the GSECARS Raman Lab System was supported by the NSF MRI Proposal (EAR-1531583).

Notes

The authors declare no competing financial interest.

■ ACKNOWLEDGMENTS

The *in situ* high-pressure powder XRD, single-crystal XRD, and Raman measurements were performed at GeoSoilEnviroCARS (The University of Chicago), Advanced Photon Source (APS), Argonne National Laboratory (ANL). This research used resources of APS, a U.S. Department of Energy (DOE) Office of Science User Facility operated for the DOE Office of Science by ANL under Contract DE-AC02-06CH11357. The authors appreciate the language editing by Freyja O'Toole.

■ REFERENCES

(1) Mao, L.; Stoumpos, C. C.; Kanatzidis, M. G. Two-Dimensional Hybrid Halide Perovskites: Principles and Promises. *J. Am. Chem. Soc.* **2019**, *141* (3), 1171−1190.
(2) Katan, C.; Mercier, N.; Even, J. Quantum and Dielectric Confinement Effects in Lower-Dimensional Hybrid Perovskite Semiconductors. *Chem. Rev.* **2019**, *119* (5), 3140−3192.
(3) Jena, A. K.; Kulkarni, A.; Miyasaka, T. Halide Perovskite Photovoltaics: Background, Status, and Future Prospects. *Chem. Rev.* **2019**, *119* (5), 3036−3103.
(4) Cao, D. H.; Stoumpos, C. C.; Farha, O. K.; Hupp, J. T.; Kanatzidis, M. G. 2D Homologous Perovskites as Light-Absorbing Materials for Solar Cell Applications. *J. Am. Chem. Soc.* **2015**, *137* (24), 7843−7850.
(5) Tsai, H.; Nie, W.; Blancon, J.-C.; Stoumpos, C. C.; Asadpour, R.; Harutyunyan, B.; Neukirch, A. J.; Verduzco, R.; Crochet, J. J.; Tretiak, S.; Pedesseau, L.; Even, J.; Alam, M. A.; Gupta, G.; Lou, J.; Ajayan, P. M.; Bedzyk, M. J.; Kanatzidis, M. G.; Mohite, A. D. High-efficiency two-dimensional Ruddlesden-Popper perovskite solar cells. *Nature* **2016**, *536* (7616), 312−316.
(6) Blancon, J.-C.; Tsai, H.; Nie, W.; Stoumpos, C. C.; Pedesseau, L.; Katan, C.; Kepenekian, M.; Soe, C. M. M.; Appavoo, K.; Sfeir, M. Y.; Tretiak, S.; Ajayan, P. M.; Kanatzidis, M. G.; Even, J.; Crochet, J. J.; Mohite, A. D. Extremely efficient internal exciton dissociation through edge states in layered 2D perovskites. *Science* **2017**, *355* (6331), 1288−1292.
(7) Fu, Y.; Zhu, H.; Chen, J.; Hautzinger, M. P.; Zhu, X. Y.; Jin, S. Metal halide perovskite nanostructures for optoelectronic applications and the study of physical properties. *Nat. Rev. Mater.* **2019**, *4* (3), 169−188.
(8) Milot, R. L.; Sutton, R. J.; Eperon, G. E.; Haghighirad, A. A.; Martinez Hardigree, J.; Miranda, L.; Snaith, H. J.; Johnston, M. B.; Herz, L. M. Charge-Carrier Dynamics in 2D Hybrid Metal-Halide Perovskites. *Nano Lett.* **2016**, *16* (11), 7001−7007.
(9) Sum, T. C.; Mathews, N. Advancements in perovskite solar cells: photophysics behind the photovoltaics. *Energy Environ. Sci.* **2014**, *7* (8), 2518−2534.
(10) Li, J.; Yu, Q.; He, Y.; Stoumpos, C. C.; Niu, G.; Trimarchi, G. G.; Guo, H.; Dong, G.; Wang, D.; Wang, L.; Kanatzidis, M. G. Cs2PbI2Cl2, All-Inorganic Two-Dimensional Ruddlesden-Popper Mixed Halide Perovskite with Optoelectronic Response. *J. Am. Chem. Soc.* **2018**, *140* (35), 11085−11090.
(11) Ji, C.; Li, B.; Liu, W.; Smith, J. S.; Majumdar, A.; Luo, W.; Ahuja, R.; Shu, J.; Wang, J.; Sinogeikin, S.; Meng, Y.; Prakapenka, V. B.; Greenberg, E.; Xu, R.; Huang, X.; Yang, W.; Shen, G.; Mao, W. L.; Mao, H.-K. Ultrahigh-pressure isostructural electronic transitions in hydrogen. *Nature* **2019**, *573* (7775), 558−562.
(12) Lu, X.; Yang, W.; Jia, Q.; Xu, H. Pressure-induced dramatic changes in organic-inorganic halide perovskites. *Chem. Sci.* **2017**, *8* (10), 6764−6776.
(13) Wang, Y.; Guo, S.; Luo, H.; Zhou, C.; Lin, H.; Ma, X.; Hu, Q.; Du, M.-h.; Ma, B.; Yang, W.; Lü, X. Reaching 90% Photoluminescence Quantum Yield in One-Dimensional Metal Halide C4N2H14PbBr4 by Pressure-Suppressed Nonradiative Loss. *J. Am. Chem. Soc.* **2020**, *142* (37), 16001−16006.
(14) Wang, Z.; Wen, X. D.; Hoffmann, R.; Son, J. S.; Li, R.; Fang, C. C.; Smilgies, D. M.; Hyeon, T. Reconstructing a solid-solid phase transformation pathway in CdSe nanosheets with associated soft ligands. *Proc. Natl. Acad. Sci. U. S. A.* **2010**, *107* (40), 17119−17124.
(15) Lü, X.; Stoumpos, C.; Hu, Q.; Ma, X.; Zhang, D.; Guo, S.; Hoffman, J.; Bu, K.; Guo, X.; Wang, Y.; Ji, C.; Chen, H.; Xu, H.; Jia, Q.; Yang, W.; Kanatzidis, M. G.; Mao, H.-K. Regulating off-centering distortion maximizes photoluminescence in halide perovskites. *Natl. Sci. Rev.* **2020**, nwaa288.
(16) Wang, Z.; Schliehe, C.; Wang, T.; Nagaoka, Y.; Cao, Y. C.; Bassett, W. A.; Wu, H.; Fan, H.; Weller, H. Deviatoric stress driven formation of large single-crystal PbS nanosheet from nanoparticles and in situ monitoring of oriented attachment. *J. Am. Chem. Soc.* **2011**, *133* (37), 14484−14487.

(17) Bai, F.; Bian, K.; Huang, X.; Wang, Z.; Fan, H. Pressure Induced Nanoparticle Phase Behavior, Property, and Applications. *Chem. Rev.* **2019**, *119*, 7673−7717.
(18) Lü, X.; Yang, W.; Quan, Z.; Lin, T.; Bai, L.; Wang, L.; Huang, F.; Zhao, Y. Enhanced Electron Transport in Nb-Doped TiO_2 Nanoparticles via Pressure-Induced Phase Transitions. *J. Am. Chem. Soc.* **2014**, *136* (1), 419−426.
(19) Li, M.; Liu, T.; Wang, Y.; Yang, W.; Lü, X. Pressure responses of halide perovskites with various compositions, dimensionalities, and morphologies. *Matter Radiat. Extremes* **2020**, *5* (1), 018201.
(20) Yin, T.; Liu, B.; Yan, J.; Fang, Y.; Chen, M.; Chong, W. K.; Jiang, S.; Kuo, J. L.; Fang, J.; Liang, P.; Wei, S.; Loh, K. P.; Sum, T. C.; White, T. J.; Shen, Z. X. Pressure-Engineered Structural and Optical Properties of Two-Dimensional (C4H9NH3)2PbI4 Perovskite Exfoliated nm-Thin Flakes. *J. Am. Chem. Soc.* **2019**, *141* (3), 1235−1241.
(21) Liu, G.; Kong, L.; Guo, P.; Stoumpos, C. C.; Hu, Q.; Liu, Z.; Cai, Z.; Gosztola, D. J.; Mao, H.-k.; Kanatzidis, M. G.; Schaller, R. D. Two Regimes of Bandgap Red-Shift and Partial Ambient Retention in Pressure-Treated Two-Dimensional Perovskites. *ACS Energy Lett.* **2017**, *2* (11), 2518−2524.
(22) Liu, S.; Sun, S.; Gan, C. K.; Del Aguila, A. G.; Fang, Y.; Xing, J.; Do, T. T. H.; White, T. J.; Li, H.; Huang, W.; Xiong, Q. Manipulating efficient light emission in two-dimensional perovskite crystals by pressure-induced anisotropic deformation. *Sci. Adv.* **2019**, *5* (7), eaav9445.
(23) Jaffe, A.; Lin, Y.; Mao, W. L.; Karunadasa, H. I. Pressure-induced conductivity and yellow-to-black piezochromism in a layered Cu-Cl hybrid perovskite. *J. Am. Chem. Soc.* **2015**, *137* (4), 1673−1678.
(24) Guo, S.; Zhao, Y.; Bu, K.; Fu, Y.; Luo, H.; Chen, M.; Hautzinger, M. P.; Wang, Y.; Jin, S.; Yang, W.; Lu, X. Pressure-Suppressed Carrier Trapping Leads to Enhanced Emission in Two-Dimensional Perovskite (HA)2(GA)Pb2I7. *Angew. Chem., Int. Ed.* **2020**, *59*, 17533−17539.
(25) Zeng, Q.; Wang, K.; Qiao, Y.; Li, X.; Zou, B. Negative Linear Compressibility Due to Layer Sliding in a Layered Metal-Organic Framework. *J. Phys. Chem. Lett.* **2017**, *8* (7), 1436−1441.
(26) Liu, G.; Gong, J.; Kong, L.; Schaller, R. D.; Hu, Q.; Liu, Z.; Yan, S.; Yang, W.; Stoumpos, C. C.; Kanatzidis, M. G.; Mao, H. K.; Xu, T. Isothermal pressure-derived metastable states in 2D hybrid perovskites showing enduring bandgap narrowing. *Proc. Natl. Acad. Sci. U. S. A.* **2018**, *115* (32), 8076−8081.
(27) Chen, Y.; Fu, R.; Wang, L.; Ma, Z.; Xiao, G.; Wang, K.; Zou, B. Emission enhancement and bandgap retention of a two-dimensional mixed cation lead halide perovskite under high pressure. *J. Mater. Chem. A* **2019**, *7* (11), 6357−6362.
(28) Zhang, L.; Wu, L.; Wang, K.; Zou, B. Pressure-Induced Broadband Emission of 2D Organic-Inorganic Hybrid Perovskite (C_6H_5C2H4NH3)2PbBr4. *Adv. Sci.* **2019**, *6* (2), 1801628.
(29) Zeng, Q.; Wang, K.; Zou, B. Large Negative Linear Compressibility in InH(BDC)(2) from Framework Hinging. *J. Am. Chem. Soc.* **2017**, *139* (44), 15648−15651.
(30) Stoumpos, C. C.; Cao, D. H.; Clark, D. J.; Young, J.; Rondinelli, J. M.; Jang, J. I.; Hupp, J. T.; Kanatzidis, M. G. Ruddlesden−Popper Hybrid Lead Iodide Perovskite 2D Homologous Semiconductors. *Chem. Mater.* **2016**, *28* (8), 2852−2867.
(31) Li, S.; Luo, J.; Liu, J.; Tang, J. Self-Trapped Excitons in All-Inorganic Halide Perovskites: Fundamentals, Status, and Potential Applications. *J. Phys. Chem. Lett.* **2019**, *10* (8), 1999−2007.
(32) Smith, M. D.; Karunadasa, H. I. White-Light Emission from Layered Halide Perovskites. *Acc. Chem. Res.* **2018**, *51* (3), 619−627.
(33) Takagi, H.; Kunugita, H.; Ema, K. Influence of the image charge effect on excitonic energy structure in organic-inorganic multiple quantum well crystals. *Phys. Rev. B: Condens. Matter Mater. Phys.* **2013**, *87*, 125421.
(34) Hong, X.; Ishihara, T.; Nurmikko, A. V. Dielectric confinement effect on excitons in PbI4-based layered semiconductors. *Phys. Rev. B: Condens. Matter Mater. Phys.* **1992**, *45* (12), 6961−6964.
(35) Tanaka, K.; Takahashi, T.; Ban, T.; Kondo, T.; Uchida, K.; Miura, N. Comparative study on the excitons in lead-halide-based perovskite-type crystals CH3NH3PbBr3 CH3NH3PbI3. *Solid State Commun.* **2003**, *127*, 619−623.
(36) Jong, U.-G.; Yu, C.-J.; Ri, J.-S.; Kim, N.-H.; Ri, G.-C. Influence of halide composition on the structural, electronic, and optical properties of mixed CH3NH3Pb(I1-xBrx)3 perovskites calculated using the virtual crystal approximation method. *Phys. Rev. B: Condens. Matter Mater. Phys.* **2016**, *94* (12), 125139.
(37) Xu, Z.; Chen, M.; Liu, S. F. Layer-Dependent Ultrahigh-Mobility Transport Properties in All-Inorganic Two-Dimensional Cs2PbI2Cl2 and Cs2SnI2Cl2 Perovskites. *J. Phys. Chem. C* **2019**, *123* (45), 27978−27985.
(38) Li, Q.; Zhang, L.; Chen, Z.; Quan, Z. Metal halide perovskites under compression. *J. Mater. Chem. A* **2019**, *7* (27), 16089−16108.
(39) Yan, H.; Ou, T.; Jiao, H.; Wang, T.; Wang, Q.; Liu, C.; Liu, X.; Han, Y.; Ma, Y.; Gao, C. Pressure Dependence of Mixed Conduction and Photo Responsiveness in Organolead Tribromide Perovskites. *J. Phys. Chem. Lett.* **2017**, *8* (13), 2944−2950.
(40) Miyata, A.; Mitioglu, A.; Plochocka, P.; Portugall, O.; Wang, J. T.-W.; Stranks, S. D.; Snaith, H. J.; Nicholas, R. J. Direct measurement of the exciton binding energy and effective masses for charge carriers in organic−inorganic tri-halide perovskites. *Nat. Phys.* **2015**, *11* (7), 582−587.
(41) Blancon, J. C.; Stier, A. V.; Tsai, H.; Nie, W.; Stoumpos, C. C.; Traore, B.; Pedesseau, L.; Kepenekian, M.; Katsutani, F.; Noe, G. T.; Kono, J.; Tretiak, S.; Crooker, S. A.; Katan, C.; Kanatzidis, M. G.; Crochet, J. J.; Even, J.; Mohite, A. D. Scaling law for excitons in 2D perovskite quantum wells. *Nat. Commun.* **2018**, *9* (1), 2254.
(42) Yuan, M.; Quan, L. N.; Comin, R.; Walters, G.; Sabatini, R.; Voznyy, O.; Hoogland, S.; Zhao, Y.; Beauregard, E. M.; Kanjanaboos, P.; Lu, Z.; Kim, D. H.; Sargent, E. H. Perovskite energy funnels for efficient light-emitting diodes. *Nat. Nanotechnol.* **2016**, *11* (10), 872−877.

https://dx.doi.org/10.1021/jacs.0c11730
J. Am. Chem. Soc. 2021, 143, 2545−2551